Laser and Particle Beams (2001), *19*, 91–97. Printed in the USA.

Characterization of electron beam propagation through foils by innershell X-ray spectroscopy

G. PRETZLER,[1,2] TH. SCHLEGEL,[3] AND E. FILL[1]

[1]Max-Planck-Institut für Quantenoptik, D-85748 Garching, Germany
[2]Sektion Physik, Universität München, D-85748, Garching, Germany
[3]Gesellschaft für Schwerionenforschung, D-64291 Darmstadt, Germany

(RECEIVED 30 November 2000; ACCEPTED 5 February 2001)

Abstract

Characteristic X-rays generated by high-intensity laser interaction with solids were investigated and used for determining the resulting hot electron populations. Spectrally as well as spatially resolved data are evaluated for this purpose. The experimental data were compared with Monte Carlo simulations to determine the electron energy distribution and geometric features of the electron beam. These results are in good agreement with PIC simulations. The self-generated low-resistivity channel of the electron beam results in a distinct difference in the generated rear-side X-ray spot when the electron beam propagates in an insulator rather than a metal. Self-generated electric fields prevent electron propagation into the vacuum. This fact is used for demonstrating photopumping of cobalt with copper K_α radiation, an experiment relevant to innershell X-ray laser schemes. The emission of cobalt is compared with that of nickel, which is not photopumped by copper K_α, and is found to be enhanced by a factor of 2.5.

1. INTRODUCTION

It has long been known that electrons with very high temperatures are generated when a high-intensity laser beam interacts with a solid target (see, e.g., Forslund *et al.*, 1977; Estabrook & Kruer, 1982; Luther-Davies *et al.*, 1987). In recent years, the invention of CPA lasers generating ultrashort pulses (Maine *et al.*, 1988) has triggered intense investigations of this effect (Davies *et al.*, 1997; Tatarakis *et al.*, 1998; Cowan *et al.*, 1999). Moreover, increasing interest in hot-electron generation is derived from proposal of the fast ignitor for inertial confinement fusion (Tabak *et al.*, 1994), observation of ion beams behind solid targets (Clark *et al.*, 2000; Snavely *et al.*, 2000), and generation and application of intense, ultrashort X-ray pulses (Rose-Petruck *et al.*, 1999), and X-ray lasers (Fill *et al.*, 1999).

The electrons propagate into the target and generate hard X-rays consisting of bremsstrahlung and characteristic radiation. Analysis of this radiation can be used to determine properties of the electron beam such as its energy distribution and directionality (Hares *et al.*, 1979; Luther-Davies *et al.*, 1987; Wharton *et al.*, 1998; Eder *et al.*, 2000).

Address correspondence and reprint requests to: Dr. E. Fill, Max-Planck Institut für Quantenoptik, Hans-Kopfermann-Str. 1, D-85748 Garching, Germany. E-mail: erf@mpq.mpg.de.

In this paper, first we present results obtained at our laboratory on the characteristic X-ray emission from the rear side of copper targets and on the properties of the electrons propagating into the target. Then we report new observations on propagation of the electron beam in conducting and nonconducting media, demonstrating the influence of self-generated *magnetic* fields on electron propagation. Furthermore, self-generated *electric* fields are shown to prevent the electron beam from emerging from the solid. This fact is used to demonstrate photopumping of K_α radiation in cobalt by copper X-rays generated in the primary target.

2. EXPERIMENTAL ARRANGEMENT

Titanium–sapphire laser pulses with a pulse duration of 130 fs and an energy of 200 mJ were focused to a spot 10 μm in diameter on solid targets by means of an off-axis parabola (Fig. 1). The peak intensity reached at best focus was 2×10^{18} W/cm^2. The laser pulse is applied p-polarized at 45° to the target. A small spurious prepulse generates a preplasma with a scale length $L/\lambda \approx 0.7$. An X-ray CCD in the energy readout mode (Dunn *et al.*, 1995) was used for spectrally resolved detection with a resolution of 200 eV, sufficient to separate the K_α lines of the different materials. To obtain the spatially resolved X-ray emission, a steel wedge was inserted between the target and detector.

https://doi.org/10.1017/S0263034601191147 Published online by Cambridge University Press

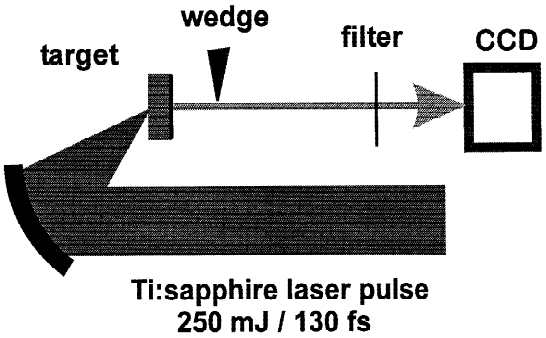

Fig. 1. Experimental arrangement used for investigating hot-electron generation. 250-mJ/130-fs titanium–sapphire laser pulses are focused on the targets by means of an off-axis parabola. To obtain spatial resolution, a stainless-steel wedge is inserted between the emitter and the CCD. A 100-μm beryllium filter blocks soft X-rays. The CCD used to detect rear-side nickel K_α emission has a 15-μm cobalt filter.

Copper foils of various thicknesses, backed by a thin nickel foil, were used to characterize the electrons propagating into the target. Nickel is not photopumped by copper K_α radiation and its emission thus serves as an indicator of the electrons arriving at the back of the copper foil. These targets were made by galvanically depositing one material on the other. This procedure was found to be necessary to prevent spurious fields from being generated at the interface between the two materials.

3. ELECTRON ENERGY DISTRIBUTION

A thorough analysis of the electron energy distribution was made by using the X-ray emission from the rear side of composite targets. Copper foils up to 43 μm thick were backed by a 10-μm nickel foil. The results obtained for the intensity of nickel K_α are shown in Figure 4. Going from 2 μm of copper to a 10-μm copper layer reduces the emission by a factor of about five, but from then on, it decreases only slowly with increasing copper foil thickness.

These data are well reproduced by Monte Carlo electron-photon transport simulations as also shown in Figure 2. For these simulations the TIGER/ITS Monte Carlo electron-photon transport code was used (Seltzer, 1991). We use version 3.0 of the ITS package, which was released in 1992. The code tracks individual electrons and treats all collisional and radiative interactions with cold material. Electric field effects are not taken into account in the simulations, a fact well justified by the high conductivity of copper and the high collisionality of the medium-Z material (see, however, Section 4).

The steep drop of the emission after the first 10 μm of copper and the persistence of the signal over the next 50 μm suggested a two-temperature distribution of the electrons propagating into the cold material. A good fit was obtained with 97% of the electrons having a temperature of 20 keV and 3% having 200 keV.

This "experimental" electron energy distribution can be compared with that obtained by PIC simulations. With the $1\frac{1}{2}$-D EUTERPE code developed at LULI (Bonnand & Reisse, 1986), a two-temperature distribution is also obtained. The electron energy distribution is as shown in Figure 3. At 2×10^{18} W/cm^2, the temperatures are 200 keV and 40 keV with an approximately equal number of electrons in the two distributions. The higher temperature thus corresponds well to the experimental one, whereas the lower temperature is a factor of two higher and the number of electrons in the lower temperature distribution is much too

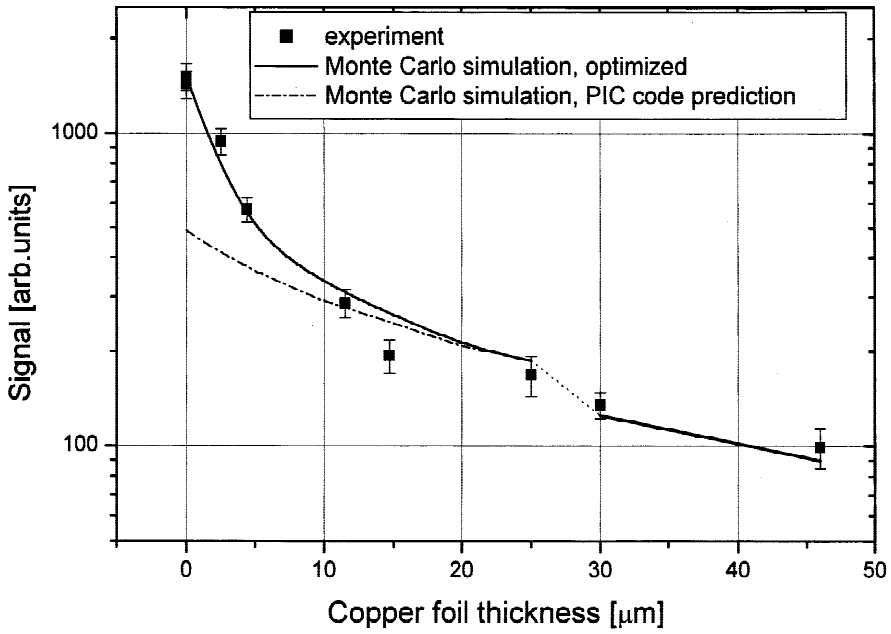

Fig. 2. Ni K_α signal versus Cu foil thickness. The error bars include statistical shot-to-shot fluctuation from seven shots. The solid line is the result obtained from TIGER Monte Carlo simulations with an electron population (97% 20 keV electrons and 3% 200 keV electrons) fitting the data. The break between 25 μm and 30 μm is due to slightly different thickness of the nickel layer resulting from different target fabrication procedures used for small and large copper foil thicknesses. The dot-dashed line is obtained by using the PIC code result in the TIGER simulations. To reproduce the initial steep drop, the 20 keV population is required.

https://doi.org/10.1017/S0263034601191147 Published online by Cambridge University Press

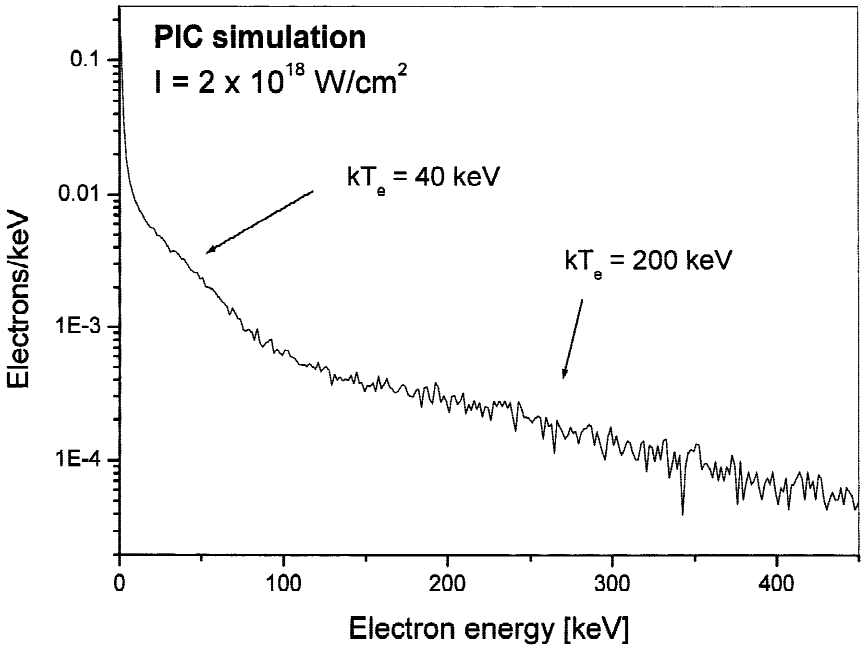

Fig. 3. Electron energy distributions as obtained by PIC code simulations. The curves exhibit two straight portions to which temperatures (40 keV and 200 keV with about equal populations for each temperature) can be ascribed.

low. This difference in the results of simulation and experiment can be explained by the intensity distribution in the focal spot (Pretzler *et al.*, 2000).

It is noted that the higher electron temperature of the two agrees well with the electron temperatures reported in experiments of other laboratories (see the review by Gibbon & Förster, 1996) which resulted in a scaling law given by Beg *et al.* (1997):

$$kT \approx 100[I_{17}\lambda_1^2]^{1/3}\ \text{keV}, \tag{1}$$

where I_{17} is the laser intensity in 10^{17} W/cm^2 and λ_1 is the laser wavelength in microns.

Absolute calibration of the CCD by means of a radioactive source of Fe^{55} emitting a known amount of Mn^{55} K_α-radiation at 5.9 keV made it possible to determine the absolute number of electrons. We obtain 1.0×10^9 Ni K_α photons emitted behind 46 μm of copper. The number of K_α photons per electron obtained from the TIGER code then results in an absolute number of $(9 \pm 3) \times 10^{11}$ electrons with a temperature of 200 keV and an energy conversion efficiency of 14% into these electrons. These data can be used to derive a total current of $I = 500$ kA obtained in the interaction. This current exceeds the so-called Alfvén current (Alfvén, 1939)

$$I_A = 17.4\beta\gamma\ \text{kA} \tag{2}$$

by more than an order of magnitude. The Alfvén current is derived as the limiting current in vacuum due to electron deflection by the magnetic field of the beam itself. However, in a solid, a strong return current is generated (Hammer & Rostoker, 1970; Lee & Sudan, 1971) which neutralizes the greater part of the magnetic field, making propagation of much higher currents possible.

4. SPOT SIZE OF THE REAR-SIDE EMISSION

To test the validity of the purely collisional model used in the Monte Carlo simulations under different conditions, electron propagation in metals was compared with that in an insulator. For this purpose, the size of the X-ray emission at the back of the targets was measured by means of the half-shadow method. For the metal targets, copper and aluminum foils with thicknesses of up to 100 μm were used. The insulator target consisted of a 1-μm aluminum foil followed by 100 μm of quartz. All of these targets were backed by a 10-μm nickel foil, the K_α radiation of which served as an indicator of the electrons propagating through the solid.

The results of these measurements are summarized in Figure 4, which shows the measured full width at half maximum (FWHM) spot sizes as a function of the material thickness through which the electrons propagated. The spot sizes obtained from the Monte Carlo simulations for copper and quartz are also shown. First we note that the spot size even at short distances is considerably larger than the laser spot size. Similar behavior was found also for the spot size of the front side emission and was attributed to hot electrons generated in the wings of the focal spot and to electrons making spurious orbits in front of the target (Eder *et al.*, 2000).

Inspecting the results for different foil thicknesses, it is seen that in copper the collisional model results in a good match between the experimental and theoretical spot sizes. For aluminum—assuming a similar electron population—one would expect to see a spot size which is smaller than the

https://doi.org/10.1017/S0263034601191147 Published online by Cambridge University Press

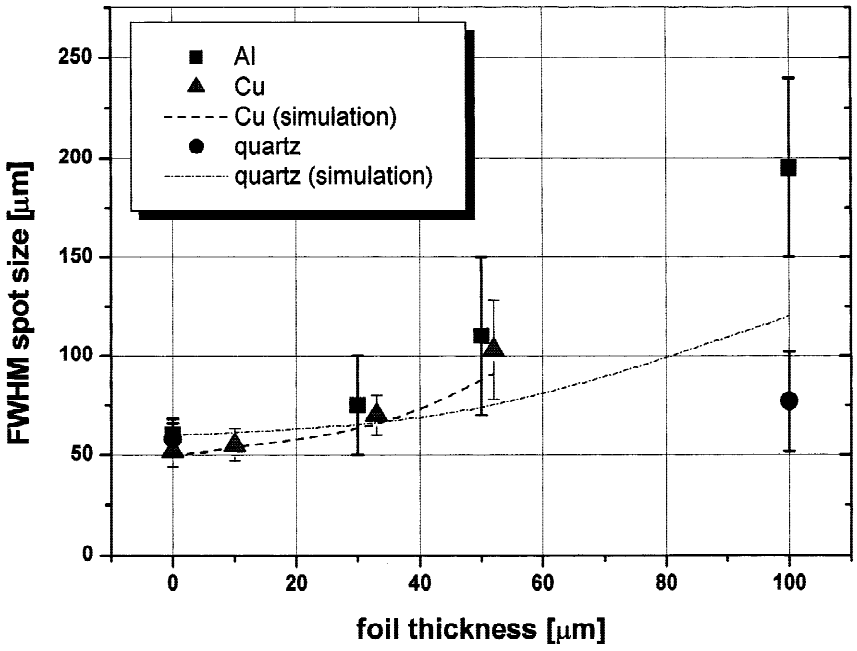

Fig. 4. Spot size of Ni K_α emission at the back of different targets. The figure displays data for electrons propagating in copper, aluminum and quartz. The copper data approximately agree with Monte Carlo simulations. The quartz spot size is significantly smaller than predicted by simulations indicative of magnetic field effects.

one of copper due to the reduced collisionality of the lower-Z material. However, our data show that the increase in spot size with increasing foil thickness is quite similar. This can be explained either by assuming that the temperature of hot electrons generated in aluminum is significantly lower than that for copper. We note that a change of mean electron energy with target material has been reported (Wharton *et al.*, 1998). Their data at 2×10^{19} W/cm^2 could be fitted with mean energies $E_0 = 120$ keV for carbon, $E_0 = 330$ keV for aluminum, and $E_0 = 640$ keV for copper. Reducing our electron temperature obtained for copper (200 keV) by a similar factor for aluminum resulted in a spot size which was still lower than that measured, but already inside the error bar. A different way to match Monte Carlo simulations to the aluminum data would be to assume a wider angular spread of the generated electron beam. Unfortunately, the available data do not allow a distinction between the two possible explanations to be made.

For quartz, the spot size experimentally obtained is much smaller than that predicted by the collisional model. This finding is in keeping with recent observations of collimated electron jets propagating in quartz (Borghesi *et al.*, 1999; Gremillet *et al.*, 1999). The difference in the behavior of a conductor and an insulator is explained by the formation of a low-resistivity channel in an insulator which enhances collimation of the electron beam (Davies *et al.*, 1999).

5. INNERSHELL PHOTOPUMPING OF COBALT BY COPPER K_α

A proposal for an X-ray laser operating in the kiloelectron volt X-ray region involves generation of an inversion by photoionization of *K*-shell holes (Duguay & Rentzepis, 1967). Inversion on innershell transitions can only be achieved by photopumping, whereas the electrons, due to their much larger cross section for the ionization of outer shells, have a higher probability of generating *L*-holes, which constitute the lower level of the K_α transition.

In view of this problem, methods have to be found to prevent hot electrons from reaching the medium to be pumped. This can be achieved by sandwiching a low-Z material between pump and pumped medium (Fill *et al.*, 2000). However, efficiently blocking high energy electrons requires at least 1 mm of low-Z absorber and thus the intensity of the pumping X-rays is much reduced.

In this work, we took advantage of the fact that self-generated fields of an electron beam hinder its propagation into a vacuum. This is illustrated in Figure 5, which shows the result of a PIC simulation of a monoenergetic electron beam emerging from a perfect conductor into vacuum. The current is assumed to rise instantaneously to a constant value. The figure shows space–time trajectories of the electrons. It is seen that the very first electrons escape unaffected from the solid. However, as more and more space charge builds up, the electrons are held back by the fields until finally, electrons are pulled back to the conducting solid.

Up to the time at which the first electron stops, this problem can be solved analytically (Poukey & Rostoker, 1971). The time at which this happens is given by

$$t_r = 2\sqrt{\gamma}/\omega_p, \tag{3}$$

and the maximum distance of this electron from the target is

$$x_r = (c/\omega_p)(\gamma - 1)/\beta\sqrt{\gamma}, \tag{4}$$

https://doi.org/10.1017/S0263034601191147 Published online by Cambridge University Press

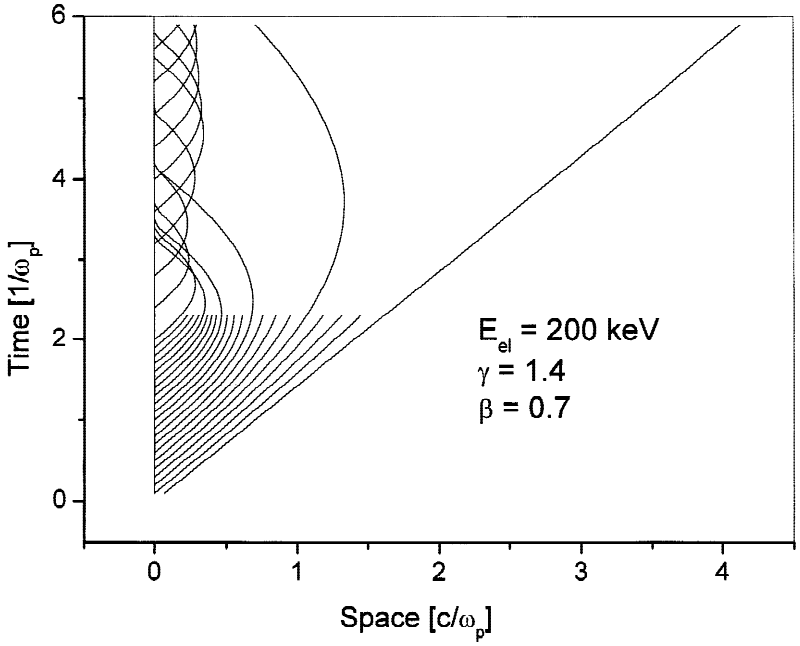

Fig. 5. Spatiotemporal trajectories of electrons emerging from a perfect conductor into vacuum. The parameters of the electron beam are indicated. Up to a time of $2.4/\omega_p$ every 100th electron trajectory is shown; after that time, for clarity, the trajectory of only every 400th electron is displayed.

where γ is the relativistic mass factor of the electrons, β is the velocity of electrons divided by c and $\omega_p = (4\pi e^2 n_b/m)^{1/2}$ is the plasma frequency of the beam electrons, n_b is the electron density in the beam and m is the electron mass. With the data of the electron beam, one obtains a beam plasma frequency of $1.6 \times 10^{14}\ s^{-1}$. The parameters β and γ are not well defined for a beam with a distribution of energies. Using 200 keV for the electron energy, the time for building up the space charge field is calculated to be approximately 15 fs and the first returning electron stops at a distance of about 1 μm from the target. The PIC simulation shows that the space charge field generates an electron sheet at a distance of about $0.4\ c/\omega_p$ from the solid.

Innershell photopumping was demonstrated in an experiment using a double-foil target. A 10-μm copper foil irradiated by intense laser pulses generates pump radiation consisting of K_α, K_β, and bremsstrahlung. A 10-μm cobalt foil is placed a short distance behind the copper and irradiated by the copper X-rays. A thin vacuum gap separates the cobalt and copper foils from each other and thus electrons are held back by self-generated fields. The amount of photopumping is assessed by comparing the emission of cobalt with that of nickel, which is not photopumped by copper K_α since its photon energy is below the nickel K edge.

The result of the experiment is shown in Figure 6, which compares the spectra obtained with the cobalt and nickel foils using a vacuum gap of 500 μm. Comparison of the two shows enhancement of the Co K_α emission with respect to the Ni K_α emission by a factor of 2.5. From the considerations above with reduced separation of the two foils, a similar result should still be obtained. This is demonstrated in Figure 7 which shows the K_α-cobalt to K_α-nickel ratio as a function of the spacing between the two foils. Down to a distance of 100 μm, this ratio is approximately constant. However, if the cobalt and nickel foils are in immediate contact with the copper foil, the enhancement of the cobalt radiation is found to be only 20%.

The foregoing results demonstrate that a thin vacuum gap behind the first foil indeed prevents a great part of the electrons from reaching the second foil. If all of the nickel emission was pumped by the electrons, a Co/Ni K_α ratio of 2.5 would mean that 60% of the cobalt emission is photopumped. However, analysis using the Monte Carlo simulations reveals that about 40% of the nickel K_α emission is also photopumped, namely, that generated by bremsstrahlung and by copper K_β radiation (which is just above the nickel K edge). Taking this into account, one arrives at a total photopumped fraction in cobalt of 75%.

A second correction takes into account that photopumping is subject to opacity effects of the pump radiation and generated K_α radiation: The main part of the Cu K_α pump radiation is already absorbed in the first few microns of the cobalt foil, whereas the fast electrons deposit their energy quite uniformly. Moreover, part of the Co K_α emission is self-absorbed in the 10-μm thick foil. Taking these effects into account is equivalent to calculating the photopumped fraction for the very first layer of the pumped medium. Making these corrections yields the result that at the very first layer, 91% of the cobalt K_α emission is photopumped.

Let it be said that the generation of gain still requires a higher percentage of photopumping. The cross section for L-hole generation by electrons is a factor of about 50 higher than that for K-holes. The ratio of the statistical weights of the upper and the lower lasing levels for $K_{\alpha 1}$ is 0.5 and thus

https://doi.org/10.1017/S0263034601191147 Published online by Cambridge University Press

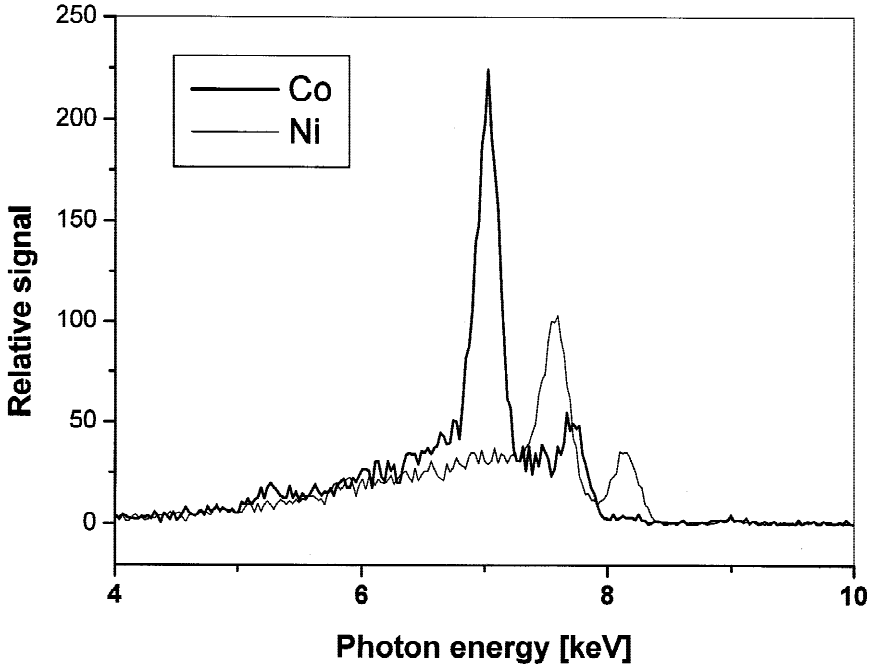

Fig. 6. Experimental spectra behind double-foil target consisting of 10 μm of copper and 10 μm cobalt or nickel separated by a 500-μm vacuum gap. The higher emission of Co K_α as compared to nickel clearly indicates photopumping. The Cu K_α pump line shines through the nickel target but is absorbed by cobalt.

roughly 96% of the *K*-holes must be photopumped in order to generate inversion.

6. CONCLUSION

Interaction of 130-fs titanium–sapphire laser pulses with copper targets at an intensity of up to 1.5×10^{18} W/cm^2 (P-polarized pulses at an angle of incidence of 45°) generates hot electrons which in turn generate hard X-rays, mainly K_α radiation.

Characterizing the hot electrons resulted in an energy distribution which can be described by two temperatures, a relatively low one of 20 keV and a fraction of 3% of the electrons with a temperature of 200 keV. Monte Carlo

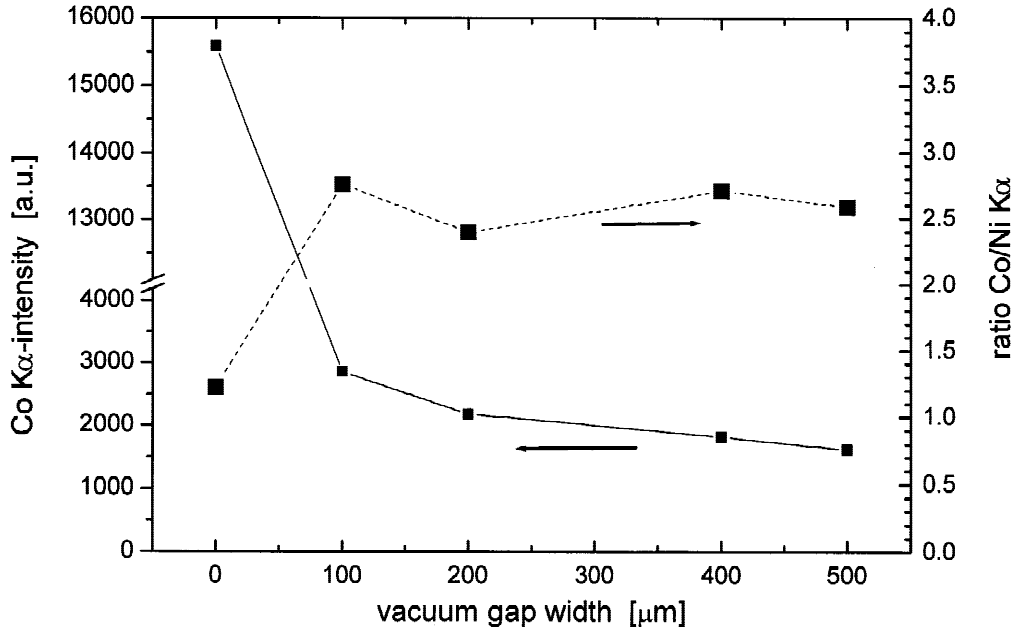

Fig. 7. Cobalt to nickel K_α ratio and Co K_α intensity versus distance between copper and backing foils. The ratio is seen to stay approximately constant to a distance down to 100 μm, while the emitted intensity increases. If the foils are in immediate contact with each other, the cobalt emission is only 20% higher than that from nickel.

https://doi.org/10.1017/S0263034601191147 Published online by Cambridge University Press

electron-photon transport simulations using these electrons at an emission angle of 30° reproduce well the intensities and spot sizes of the K_α radiation generated in a thin nickel foil backing copper foils of various thicknesses.

The X-ray emitting spot generated in a thin nickel foil was found to be significantly different in size, depending on whether the electrons propagated through aluminum or quartz. The X-ray spot size increased by a factor of three when the beam propagated through 100 μm of aluminum, whereas in the case of quartz, the X-ray spot at the same distance increased only by 25%. This result is attributed to a self-generated low-resistivity channel confining the electron beam.

An experiment demonstrating photopumping of cobalt using copper K_α radiation as the pump is conducted with a target consisting of a 10-μm copper foil irradiating a 10-μm cobalt foil. The main part of the electrons is prevented by self-generated electric fields from reaching the cobalt. This yields a photopumped fraction of 75% of the cobalt emission. At the very first surface of the cobalt layer, the photopumped fraction is 91%.

ACKNOWLEDGMENTS

A. Böswald and H. Haas are thanked for ensuring reliable operation of the ATLAS laser and W. Fölsner for fabricating the targets. We thank R. Volk for the installation of the TIGER code. This work was supported in part by the Commission of the European Communities within the framework of the Euratom/Max-Planck-Institut für Plasmaphysik Association.

REFERENCES

Alfvén, H. (1939). *Phys. Rev.* **35**, 425.
Beg, F.N. *et al.* (1997). *Phys. Plasmas* **4**, 447.
Bonnand, G. & Reisse, G. (1986). *Nucl. Fusion* **26**, 633.
Borghesi, M. *et al.* (1999). *Phys. Rev. Lett.* **83**, 4309.
Clark, E.L. *et al.* (2000). *Phys. Rev. Lett.* **84**, 670.
Cowan, T.E. *et al.* (1999). *Laser Part. Beams* **17**, 773.
Davies, J.R. *et al.* (1997). *Phys. Rev. E* **56**, 7193.
Davies, J.R., Bell, A.R. & Tatarakis, M. (1999). *Phys. Rev. E* **59**, 6032.
Duguay, M.A. & Rentzepis, P.M. (1967). *Appl. Phys. Lett.* **10**, 350.
Dunn, J. *et al.* (1995). *Rev. Sci. Instr.* **66**, 706.
Eder, D.C. *et al.* (2000). *Appl. Phys. B* **70**, 211.
Estabrook, K. & Kruer, W.L. (1983). *Phys. Fluids* **26**, 7.
Fill, E. *et al.* (1999). *Soft X-ray Lasers and Applications III*, SPIE 3776, J.J. Rocca and L. Da Silva, eds., p. 110.
Fill, E. *et al.* (2000). In *Proc. Seventh Int. Conf. X-ray Lasers* (St. Malo, France, June 2000), A. Klisnick, ed. to be published.
Forslund, D.W., Kindel, J.M. & Lee, K. (1977). *Phys. Rev. Lett.* **39**, 284.
Gibbon, P. & Förster, E. (1996). *Plasma Phys. Contr. Fusion* **38**, 769.
Gremillet, L. *et al.* (1999). *Phys. Rev. Lett.* **83**, 5015.
Hammer, D.A. & Rostoker, N. (1970). *Phys. Fluids* **13**, 1831.
Hares, J.D. *et al.* (1979). *Phys. Rev. Lett.* **42**, 1216.
Lee, R. & Sudan, R.N. (1971). *Phys. Fluids* **14**, 1213.
Luther-Davies, B., Perry, A. & Nugent, K.D. (1987). *Phys. Rev. A* **35**, 4306.
Maine, P. *et al.* (1988). *IEEE J. Quant. Electron* **24**, 398.
Poukey, J.W. & Rostoker, N. (1971). *Plasma Phys.* **13**, 897.
Pretzler, G. *et al.* (2000). *Phys. Rev. E* **62**, 5618.
Rose-Petruck, C. *et al.* (1999). *Nature* **398**, 310.
Seltzer, S.M. (1991). *Appl. Radiat. Isot.* **42**, 917.
Snavely, R.A. *et al.* (2000). *Phys. Rev. Lett.* **85**, 2945.
Tabak, M. *et al.* (1994). *Phys. Plasmas* **1**, 1626.
Tatarakis, M. *et al.* (1998). *Phys. Rev. Lett.* **81**, 999.
Wharton, K.B. *et al.* (1998). *Phys. Rev. Lett.* **81**, 822.